An integrative model of plant gravitropism linking statoliths position and auxin transport

Nicolas Levernier [1,*], **Olivier Pouliquen** [1] **and Yoël Forterre** [1]

[1] *Aix Marseille Univ, CNRS, IUSTI, Marseille, France*

Correspondence*:
IUSTI, 5 rue Enrico Fermi, 13453 Marseille cedex 13, France
nicolas.levernier@univ-amu.fr

ABSTRACT

Gravity is a major cue for proper plant growth. The response to this cue implies starch-filled plastids, the statoliths, sedimenting on the bottom of statocytes cells. These statoliths are assumed to modify the transport of the growth hormone by acting on specific hormone carriers, PIN proteins, in an unknown way. Recent experiments show that statholiths do not act as gravitational force sensor, but as position sensor. Moreover, the signal is not immediate but integrated over a time-scale of a tens of minutes. However, the precise gravitropic signaling pathway from the sensing of this cue at the cell scale to the response in growth at the tissue scale is still not understood. Here we present a bottom-up theory that enables to rationalize the previous phenomenological results from microscopic considerations. Our approach, consistent with existing experimental results, tends to support that the integration time-scale is associated to PIN turnover. Moreover, it leads to a revision of the so-called sine-law of plant gravitropism.

Keywords: Plant tropism, gravity sensing, integrative modeling, Auxin signaling, PIN trafficking

1 INTRODUCTION

The detection of gravity by plants and the associated growth response (gravitropism) offer a fascinating illustration of multi-scale perception mechanism in a living organism (Fig. 1) (Moulia and Fournier, 2009; Morita, 2010; Toyota and Gilroy, 2013). It originates in specific cells, called statocytes, where tiny starch-accumulating amyloplasts acting as statoliths sediment under gravity at the bottom of the cells (Fig. 1 c). When the plant is inclined, the repositioning of statoliths under gravity induces a relocalisation of auxin transporters (PIN proteins) at the membrane of statocytes, which generates a lateral transport of auxin toward the lower side of the shoot or the root (Cholodni-Went hypothesis) (Fig. 1 b). In turn, this asymmetry in auxin concentration induces a differential growth across the plant organ, and thus its bending toward the gravity vector (Fig. 1 a). Since the pioneering works of Darwin, progress has been made on every steps of this gravitropic signaling pathway; yet important questions remain (Nakamura et al., 2019). In particular, it is still not clear how the first physical signal generated by the sedimentation of statoliths is converted into biochemical signals downstream, to eventually produce the growth response at the plant scale.

Recently, insights into the sensing mechanism and the transduction pathway have been obtained from experiments both at the macroscopic and microscopic level. First, the gravitropic response to permanent stimuli (inclination of the plant), the so-called sine-law of gravitropism (Sachs, 1887; Larsen, 1969; Iino et al., 1996; Galland, 2002; Dumais, 2013), was found to depend on the inclination but, surprisingly,

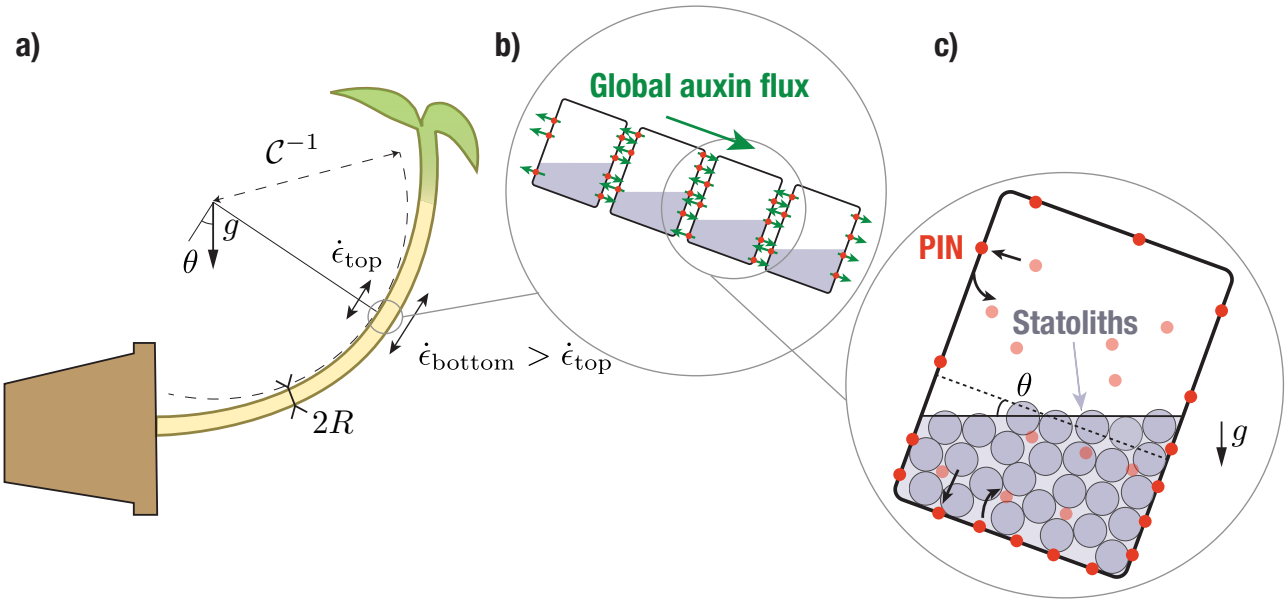

Figure 1. Multiscale description of gravitropism. At the macroscopic scale (a), the response to gravity of a shoot or a stem is achieved by differential growth across the organ, which induces a curvature of the organ. At the tissue scale (b), differential growth results from a net flux of the auxin (the growth hormone) across the width, owing to the asymmetric distribution of auxin transporters (PINs, red circles). At the cell scale (c), PIN asymmetry results from the asymmetric distribution of the statoliths position after sedimentation under gravity, which modifies PIN trafficking close to the cell membrane.

not on the intensity of gravity (Chauvet et al., 2016). Hence, statocytes behave like inclination sensors not force sensors as previously believed. An important consequence is that the initial gravity stimulus for gravitropism should be the position of the statoliths within statocytes (Pouliquen et al., 2017). This position-sensor hypothesis found mechanistic support from the direct observation of statoliths motion under gravity stimulation (Bérut et al., 2018). Unlike a pile of macroscopic grains like sand, statoliths were found to move and flow at any cell angle. This liquid-like behavior comes from the random agitation of the statoliths, whose origin is not thermal but arises from the interaction of statoliths with the acto-myosin cytoskeleton (Sack et al., 1986; Saito et al., 2005; Nakamura et al., 2011). A second observation came from dose-response like experiments on wheat coleoptiles in which the gravity stimulus is applied during a transient period only (Chauvet et al., 2019). When the shoots were inclined for short period of time, the gravitropic response was found to deviate from the steady response and strongly decay. The transition occured for a time $\tau_{\text{memory}} \sim 15$ min, which was independent of gravity and much larger than the statoliths sedimentation time. This observation suggested the existence of a memory-integration process in the gravitropic signaling pathway, independent of the statoliths dynamics, that integrates the initial signal induced by statoliths displacement.

To account for these observations (position-sensor hypothesis, memory time independent of g), Chauvet et al. (2019) built a mathematical model of gravitropism in which the gravitropic signal controlling the differential growth was linked to the statoliths position by an integrative process of timescale τ_{memory} (a similar approach was used in Meroz et al. (2019)). Once coupled to the statoliths dynamics and the tropic growth motion, the model was able to reproduce the transient gravitropic response observed experimentally. However, Chauvet et al. (2019)'s model was built on two *ad-hoc* postulates. First, it assumes that the relation between the gravitropic signal and the statoliths position is known and given by the sine-law.

Second, it postulates the existence of the integrative process and time scale τ_{memory}, without explaining its origin. To go further, one has to take into account the spatio-temporal dynamics of the molecular processes acting between the statoliths and the growth response, such as the dynamics of PIN and auxin transport.

The objective of this paper is to fill this gap by building an integrative model of plant gravitropism that bridges the different scales of the process: (i) the initial intracellular gravitropic signal encoded in the statoliths position, (ii) PIN dynamics at the cellular level, (ii) auxin transport at the tissue level and finally (iv) differential growth and curvature at the plant organ scale. Previous models of plant gravitropism mainly focused either on the macroscopic scale, describing how the complex spatio-temporal evolution of the organ shape results from the interplay between differential growth and the slender geometry of the organ (Bastien et al., 2013, 2014; Chelakkot and Mahadevan, 2017), or on the tissue level, modeling growth mechanics (Dyson et al., 2014) or auxin transport (Band et al., 2012; Fendrych et al., 2018; Retzer et al., 2019) in realistic 1D or 3D tissue geometries. In these latter models, the distribution of PINs in the statocytes in response to plant inclination was postulated and no link was made with the intracellular dynamics of the statoliths. This is precisely the goal of this study. Building on the recent position-sensor hypothesis, we propose a simple but generic model of interaction between statoliths position and PIN recycling, that we couple with the classical equation of auxin transport and tissue growth. We will then study the gravitropic response predicted by the model for steady and unsteady gravity stimuli, comparing the results with the experimental of Chauvet et al. (2016) and Chauvet et al. (2019).

2 MATERIAL AND METHODS

2.1 Link between gravitropic curvature, differential growth and auxin concentration gradient

At the plant scale, the gravitropic response is characterized by the curvature of the organ resulting from differential growth, which itself results from auxin gradients (ChodlonyWent hypothesis). The first step of the model is thus to relate those three quantities. For a slender organ like a shoot or a stem, the rate of change of the local curvature $\mathcal{C}$ is related to differential growth through the following kinematic relationship: $R\frac{d\mathcal{C}}{dt} = \frac{1}{\tau_g} \times \frac{\dot{\epsilon}_{\text{bottom}} - \dot{\epsilon}_{\text{top}}}{2\dot{\epsilon}_{\text{mean}}}$, where R is the radius of the organ, $\dot{\epsilon}_{\text{bottom}} - \dot{\epsilon}_{\text{top}}$ is the difference of growth rate between both sides , $\dot{\epsilon}_{\text{mean}}$ is the mean growth rate and $\tau_g = \dot{\epsilon}_{\text{mean}}^{-1}$ is the growth timescale Silk (1984); Moulia and Fournier (2009) (Fig. 1). The growth rate of plant cells is known to be controlled by auxin, the so-called growth hormone. Auxin stimulates cell elongation by loosening cell walls. To the best of our knowledge, the link between the local auxin concentration in walls and the local growth rate of cells has not been robustly determined and only the response of the whole tissue to an external addition of auxin from the medium has been investigated. It is however often assumed that growth is mainly controlled by the auxin concentration in the vicinity of the'skin', as epidermal tissues are stiffer than inner tissues (Kutschera and Niklas, 2007; Dyson et al., 2014). For the sake of simplicity, we will here assume that the local growth rate is simply proportional to the local auxin concentration c, $\dot{\epsilon} = kc$ Galston and Hand (1949); Hopkins and Hüner (2009), such that:

$$R\frac{d\mathcal{C}}{dt} = \frac{1}{\tau_g} \times \frac{c_{\text{bottom}} - c_{\text{top}}}{2c_{\text{mean}}}, \tag{1}$$

where c_{bottom} and c_{top} are the auxin concentrations on both sides of the organ and c_{mean} the mean auxin concentration. Under this assumption, the dimensionless gravitropic response deduced from the curvature dynamics, $\tilde{\Delta} \equiv R\tau_g \frac{d\mathcal{C}}{dt}$, is equal to the relative auxin gradient across the organ, $\tilde{\Delta} = \frac{c_{\text{bottom}} - c_{\text{top}}}{2c_{\text{mean}}}$. The goal of the model is to predict how this auxin gradient establishes when the plant is tilted.

2.2 Auxin transport

Auxin transport plays a key role in shaping plants development and, as such, has been the topic of extensive research over the past decades. Auxin transport is based on two distinct mechanisms (Goldsmith, 1977; Hopkins and Hüner, 2009; Runions et al., 2014). On the one hand, auxin in cell walls (mostly in a protonated form) enters the neighboring cell passively, or thanks to Aux/Lax influx carriers that are evenly distributed throughout the membrane. On the other hand, auxin inside cells (mostly in an anionic form) can only exit thanks to active auxin efflux carriers, such as PIN proteins (Krecek et al., 2009) or ABCB transporters (Zažímalová et al., 2010). While ABCB are evenly distributed throughout the membrane, PIN proteins are usually polarized and can be redistributed in response to external stimuli such as gravity (in particular PIN3, which is known to be implied in gravitropic response, Friml et al. (2002)). Hence, an asymmetric distribution of PIN carriers on each side of the cell can generate an active transport of auxin from one cell to the other, resulting in a stable auxin gradient.

To model this situation, we provide a simplified description of auxin transport in which the different forms of auxin (proton-associated or not) are not taken into account. The tissue across the shoot or stem (width $2R$) is modeled as a one-dimensional array of N cells of width W separated by a cell wall of width w (Fig. 1 and Fig. 2). We denote c_n the auxin concentration inside the n-th cell and C_n the auxin concentration inside the n-th wall, which are both assumed uniform (the equilibrium time of auxin in each compartment is very fast, about 0.1 s in the cell wall and few s inside the cell taking typical values of auxin diffusion coefficients, Kramer et al. (2007)). We also neglect auxin dilution due to cell growth and assume that auxin is neither degraded nor created, as the degradation time of auxin (of the order of the day, Grieneisen et al. (2012)) is much longer than the minutes to hours timescales we are interested in. The efflux current of auxin (number of auxin molecules per unit time and unit surface) from the n-th cell to the left wall (resp. right wall) is given by $P_n^l c_n$ (resp. $P_n^r c_n$), where P_n^l (resp. P_n^r) is the permeability of the left (resp. right) membrane (unit m/s). Conversely, the influx current of auxin from the n-th wall to both

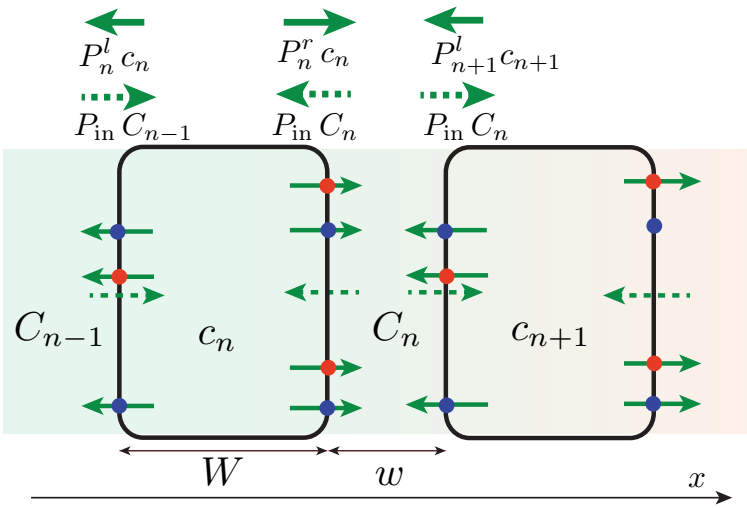

Figure 2. One-dimensional, discrete model of auxin transport across the tissue (in reality $w \ll W$). Efflux of auxin (solid green arrow) occurs through efflux carriers (PIN: red circle, ABCB: blue circle), whose distribution (and thus permeabilities $P_n^{l,r}$) can be different on the right and left membrane of the cell. By contrast, influx of auxin (green dotted arrow) occurs with a symmetrical permeability $P^{\rm in}$ on both side of the cell. An asymmetry of efflux permeabilities $P^l \neq P^r$ can generate a net flux of auxin across the tissue, yielding an auxin concentration gradient (background color gradient).

adjacent cells is $P^{\text{in}}C_n$, where the influx permeability P^{in} is assumed uniform for all cells (see Fig. 2). The time-evolution of the concentration is then:

$$w\frac{\mathrm{d}C_n}{\mathrm{d}t} = -2P^{\text{in}}C_n + P_n^r c_n + P_{n+1}^l c_{n+1}\,, \tag{2}$$

$$W\frac{\mathrm{d}c_n}{\mathrm{d}t} = -(P_n^l + P_n^r)c_n + P^{\text{in}}(C_{n-1} + C_n)\,. \tag{3}$$

The cell wall size being much smaller than the cell width ($w \ll W$), the auxin concentration in the cell wall can be assumed quasi-steady, $2P^{\text{in}}C_n \simeq P_n^r c_n + P_{n+1}^l c_{n+1}$, yielding:

$$2W\frac{\mathrm{d}c_n}{\mathrm{d}t} = P_{n+1}^l c_{n+1} - P_n^l c_n + P_{n-1}^r c_{n-1} - P_n^r c_n\,. \tag{4}$$

In the following, we assume that the distribution of auxin efflux carriers is the same in each cell, so that P^l and P^r are independent of n. This is the case of shoot coleoptiles where all cells in the growing region are similar and contain statoliths, but not the case of many stems like Arabidopsis inflorescence where statoliths are only present on an external ring in the endodermal cells (the modification of the equation in this case of inhomogeneous tissue is given in Appendix A). We also assume that auxin gradients occur over a length scale much larger than the cell size. In the continuum limit [$c_n(t) \to c(x,t)$], equation 4 for auxin transport then reduces to an advection-diffusion equation given by:

$$\frac{\partial c}{\partial t} = \mathcal{D}\frac{\partial^2 c}{\partial x^2} - v\frac{\partial c}{\partial x} \tag{5}$$

where $\mathcal{D} = WP/2$ is the coefficient of diffusion and $v = \delta P/2$ the advection speed, with $P = (P^l + P^r)/2$ and $\delta P = P^r - P^l$.

The advective part of the equation (5), which is responsible for auxin transport from one side to the other and eventually to differentiated growth and curvature of the organ, is entirely controlled by the asymmetry of efflux permeabilities δP. Since ABCB carriers are evenly distributed, this asymmetry comes from the asymmetry of PIN distribution between the right and left side of the cells:

$$\delta P = P^r - P^l = \frac{1}{S}\left(\alpha\int_S [PIN]_{|\text{right}} - \alpha\int_S [PIN]_{|\text{left}}\right), \tag{6}$$

where α is the conductance of a single PIN carrier (unit m^3/s), S the lateral surface of the cells and $[PIN]$ the surface concentration of PIN attached to the membrane. In the following, we assume that the efflux permeability due to ABCB carriers is much larger than the efflux permeability due to PIN, such that $P = (P^l + P^r)/2 \simeq (1/S)\beta\int[ABCB]$, where β is the conductance of a single ABCB carrier, is independent of PIN concentration. This enable us to take a constant coefficient of diffusion $\mathcal{D}$ in the model, which simplify the results without affecting much the conclusions.

2.3 Coupling PIN dynamics to statoliths position: biased efflux at cell scale

The previous section relates auxin transport to the asymmetry of PINs distribution at the cellular level. We now model how this asymmetry emerges when the plant is tilted under gravity. Recently, it has been demonstrated that the relevant gravitropic stimulus for graviperception is the statoliths position within the statocytes (position-sensor hypothesis), and not their weight as previously believed Chauvet et al.

(2016); Pouliquen et al. (2017). Statoliths have also been identified as key actors in the relocalisation of PIN-proteins in response to change of gravity direction Nakamura et al. (2019). Yet, how statoliths position is detected and read to modify PIN polarity remains largely unknown. PINs trafficking involves synthesis in the endoplasmic reticulum, degradation in the vacuole and recycling Kleine-Vehn and Friml (2008). Recycling is achieved by endocytosis, i.e. the deallocation of PIN proteins formerly attached to the cell membrane toward the cytoplasm inside a vesicle, or by exocytosis, i.e., the reallocation of the vesicle-carried PINs from the cytoplasm back to the cell membrane.

Following the position-sensor hypothesis, we assume that the presence of statoliths, either through direct steric constraints or through indirect molecular signaling, modify the trafficking of PIN proteins, so that PINs tend to enter the cell membrane preferentially on places where statoliths are in contact with it. This mechanism is formalized as follows. The endocytosis rate of PINs, $d[PIN]_i/dt = -k_{\text{off},i}[PIN]_i$ where $[PIN]_i$ is the surface concentration of PIN attached to the membrane, is assumed to depend on the presence of statoliths, with $i = 0$ if no statoliths are present and $i = 1$ if they are (see Fig. 3). Similarly, the rate of exocytosis is written as $d[PIN]_i/dt = +k_{\text{on},i}(N_{\text{vol}}/N_{\text{tot}})$, where N_{vol} is the number of PINs molecules inside the cell and N_{tot} the total number of PINs both inside the cell and attached to the membrane. Two cases will be distinguished in the model, depending on whether PINs can attach to any side of the cell ("apical/basal/lateral binding") or only on lateral sides ("lateral binding") (see Fig. 4 a). Assuming that the total number N_{tot} of PINs is conserved during gravistimulation (Kleine-Vehn et al., 2010) leads to the following set of equations for the PIN concentration attached to the membrane, $[PIN]_{i=0,1}$:

$$\begin{aligned}\frac{\mathrm{d}[PIN]_0}{\mathrm{d}t} &= -k_{\text{off},0}\,[PIN]_0 + k_{\text{on},0}\left(1 - \frac{S_0[PIN]_0 + S_1[PIN]_1}{N_{\text{tot}}}\right)\\ \frac{\mathrm{d}[PIN]_1}{\mathrm{d}t} &= -k_{\text{off},1}\,[PIN]_1 + k_{\text{on},1}\left(1 - \frac{S_0[PIN]_0 + S_1[PIN]_1}{N_{\text{tot}}}\right)\end{aligned} \tag{7}$$

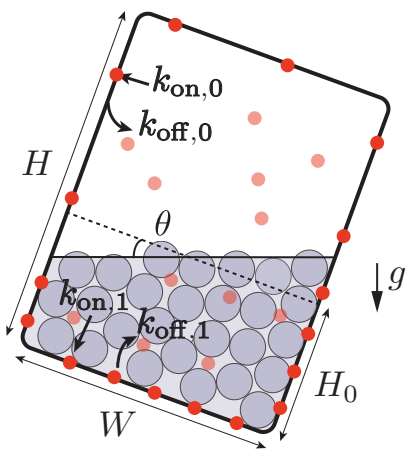

Figure 3. Interaction between PIN trafficking and statoliths position. The rate of reallocation k_{on} and deallocation k_{off} of PINs (bold red circles: PINs attached to the cell membrane, light red circles: PINs in bulk) depends on the presence of statoliths (grey).When the cell is tilted, the asymmetric distribution of the position of the statoliths induces a bias in the distribution of the PINs attached to the membrane.

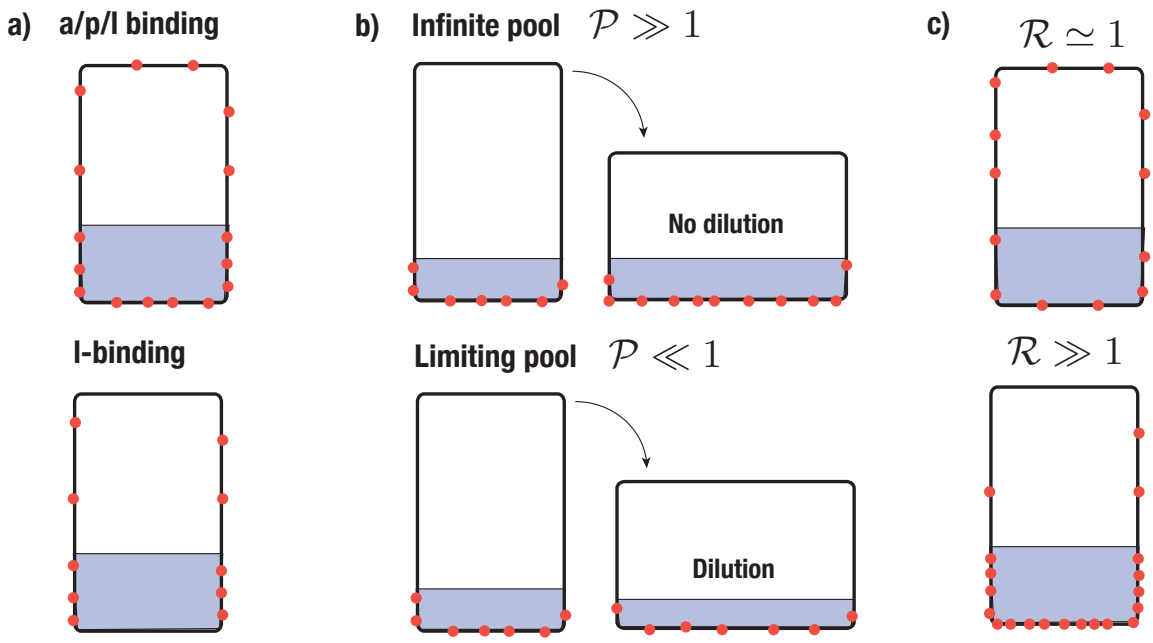

Figure 4. Sketch of different scenarii of PIN-binding. PINs are represented in red and the region with statoliths in blue. (a) Apical/basal/lateral-binding vs lateral-binding. (b) Infinite pool versus limiting pool. In the first case, the density of PIN is conserved whereas in the second one, the total number of PIN is. (c) Low sensitivity of PIN to statoliths ($\mathcal{R} \simeq 1$) or high sensitivity ($\mathcal{R} \gg 1$).

where S_1 (resp. S_0) denotes the total surface in contact (resp. not in contact) with statoliths in case of apical/basal/lateral binding, or only the lateral surfaces in contact (resp. not in contact) with statoliths in the lateral binding case.

The form of equation (7) shows that two regimes can be distinguished, depending on whether N_{tot} is large or small compared to $Sk_{\text{on}}/k_{\text{off}}$. The first regime, called "infinite-poll" regime in the following, corresponds to the case where $N_{tot}k_{\text{off}}/Sk_{\text{on}}$ is so large that binding is only limited by k_{off}. The second regime, called "limiting-pool" regime, corresponds to the opposite situation where the total number of attached carriers is strongly limited by N_{tot}, such that $S_0[PIN]_0 + S_1[PIN]_1 \simeq N_{\text{tot}}$ (see Fig. 4 b). Finally, we note that in writing Eq. (7), we have neglected the diffusion of PINs inside the membrane. This is justified since, over the time scales we are interesting in (running from minutes to one hour), PINs diffuse only over a distance of about few micrometers, which is much smaller than the cell size (taking $0.1\mu m^2$ min for the diffusion coefficient of PIN, see Kleine-Vehn et al. (2011)).

3 RESULTS

3.1 Steady gravitropic response: revisited sine-law

We first study the gravitropic response predicted by our model in the case of a steady inclination of the plant θ, for timescales long enough that the system reaches a steady state. This situation corresponds to the usual protocol for measuring the sensitivity of plant to gravity under steady condition, when the plant is suddenly inclined to a fixed angle and its curvature (or tip angle) measured over long timescale. After a transient, the rate of change of curvature is found to be constant Chauvet et al. (2016), which enables to measure the gravitropic response $\tilde{\Delta}^{\text{steady}}(\theta) = R\tau_g \frac{d\mathcal{C}}{dt}$ (see Material and Methods) for each imposed angle θ. For many plants, this relationship between the gravitropic response and the inclination angle has sine-like

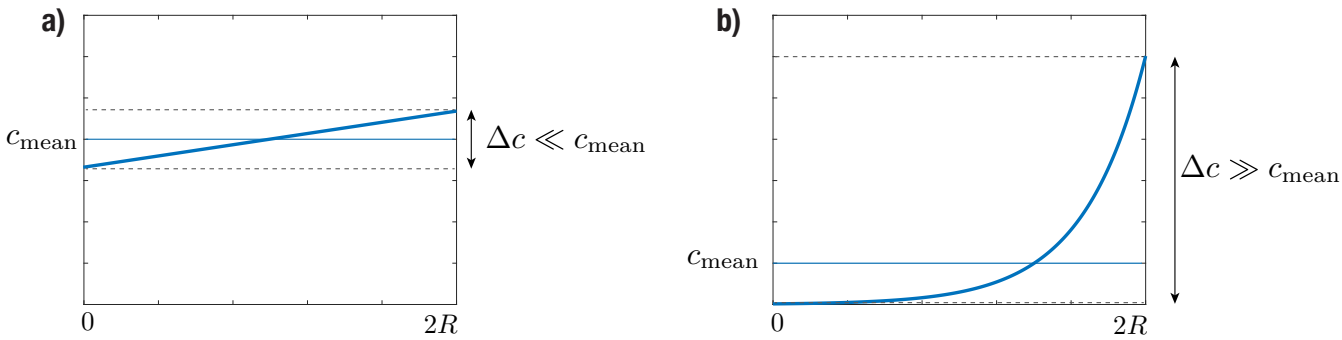

Figure 5. Stationary auxin profile for (a) small and (b) large Peclet number.

shape (the response is null for $\theta = 0°$ or $\theta = 180°$ and maximal for $\theta = 90°$) and is called the 'sine-law' of plant gravitropism in the literature (Sachs, 1887; Larsen, 1969; Iino et al., 1996; Galland, 2002; Dumais, 2013). Below, we determine the steady gravitropic response $\tilde{\Delta}^{\text{steady}}(\theta)$ predicted by the model eqs (1 , 5 , 7) and compare with measurements of the sine-law obtained previously for wheat coleoptiles over a wide range of angles Chauvet et al. (2016).

In the steady regime, the auxin transport equation (5) reduces to: $dJ/dx = 0$, where $J = \mathcal{D}(dc/dx) - vc$ is the auxin flux. For impermeable boundaries at $x = 0$ and $x = 2R$, the flux is null and the auxin concentration profile is given by:

$$c(x) = c_{\text{mean}} \frac{\text{Pe} \times \exp\left(\text{Pe}\frac{x}{2R}\right)}{\exp\left(\text{Pe}\right) - 1}, \tag{8}$$

where $c_{\text{mean}} = (1/2R)\int_0^{2R} c(x)dx$ is the mean concentration of auxin and Pe is the Peclet number given by:

$$\text{Pe} = \frac{2Rv}{\mathcal{D}} = N\frac{\delta P}{P} = N\frac{\alpha\left(\int_S [PIN]_{|\text{right}} - \int_S [PIN]_{|\text{left}}\right)}{\beta\int[ABCB]}. \tag{9}$$

For $\text{Pe} \ll 1$, the profile is linear and the auxin level in the middle of the stem is unchanged, whereas for $\text{Pe} \gg 1$ the profile is strongly asymmetric with most auxin concentrated on the right (Fig. 5). From this steady profile of auxin, the gravitropic response can be computed as $\tilde{\Delta}^{\text{steady}} = \frac{c(x=2R)-c(x=0)}{2c_{\text{mean}}}$ (eq. (1), which gives:

$$\tilde{\Delta}^{\text{steady}} = \frac{\text{Pe}}{2} \tag{10}$$

In the steady state, the gravitropic response of the plant is thus given by the value of the Peclet number. Previous measurements in various plant species representative of land angiosperm showed that $\tilde{\Delta}^{\text{steady}}$ is typically of the order 1 Chauvet et al. (2016) (for e.g. in wheat coleoptile, the maximal value of $\tilde{\Delta}^{\text{steady}}$ obtained for a 90 degrees inclination is about 0.7), meaning that the Peclet number is typically of the order 1. Therefore, the auxin profile across the shoot is expected to be close to linear (Fig. 5 a) (and not a pronounced exponential, Fig. 5 b). A consequence is that growth, which was assumed proportional to the auxin concentration, varies also linearly from one side of the shoot to the other during the gravitropic response.

The next step to determine $\tilde{\Delta}^{\text{steady}}$ is to compute the Peclet number (9), i.e., the relative distribution of PIN between the left and right side of the cell. In the steady regime, the concentration of PIN attached to a membrane not covered by statoliths ($[PIN]_0$), or covered by statoliths ($[PIN]_1$), is given by (see eq. 7):

$$[PIN]_0 = \left(\frac{k_{\text{off},0}}{k_{\text{on},0}} + \frac{1}{N_{\text{tot}}} \left[S_0 + \frac{k_{\text{on},1}\, k_{\text{off},0}}{k_{\text{on},0}\, k_{\text{off},1}} S_1 \right] \right)^{-1}$$
$$[PIN]_1 = \left(\frac{k_{\text{off},1}}{k_{\text{on},1}} + \frac{1}{N_{\text{tot}}} \left[S_1 + \frac{k_{\text{on},0}\, k_{\text{off},1}}{k_{\text{on},1}\, k_{\text{off},0}} S_0 \right] \right)^{-1} \tag{11}$$

Noting S_i^l (resp. S_i^r) the surface of the left (resp. right) side of the cell not covered ($i = 0$) or covered ($i = 1$) by statoliths, we have $\int_S [PIN]_{|\text{right}} - \int_S [PIN]_{|\text{left}} = [PIN]_0 (S_0^r - S_0^l) + [PIN]_1 (S_1^r - S_1^l)$. Finally, since $S_0^l + S_1^r = S_0^r + S_0^l = S$, where S is the lateral surface of the cells and using (9), we have:

$$\tilde{\Delta}^{\text{steady}} = \frac{\alpha N (\mathcal{R} - 1)(S_1^r - S_1^l)[PIN]_0}{2\beta \int [ABCB]} \tag{12}$$

with

$$[PIN]_0 = \frac{k_{\text{on},1}}{k_{\text{off},1}\mathcal{R}} \left(1 + \mathcal{P}^{-1} \frac{S_1}{S} \left(1 + \frac{S_0}{S_1 \mathcal{R}} \right) \right)^{-1} \tag{13}$$

and:

$$\mathcal{R} = \frac{[PIN]_1}{[PIN]_0} = \frac{k_{\text{on},1}\, k_{\text{off},0}}{k_{\text{on},0}\, k_{\text{off},1}}, \qquad \mathcal{P} = \frac{N_{\text{tot}} k_{\text{off},1}}{k_{\text{on},1} S} \tag{14}$$

The expressions (12–14) show that the steady gravitropic response is proportional to $(\mathcal{R} - 1)(S_1^r - S_1^l)$. For $\theta > 0$ as in Fig. 1, the difference $(S_1^r - S_1^l)$ is positive since statoliths sediment toward the right side of the cell. Therefore, to obtain a 'normal' gravitropic response ($\tilde{\Delta}^{\text{steady}} > 0$, i.e., a larger auxin concentration at the bottom side of the shoot), the ratio $\mathcal{R}$ must be larger than 1. The parameter $\mathcal{R}$ is the ratio between the concentration of PIN in a zone with statolith and in a zone without statolith, hence the larger $\mathcal{R}$, the more PIN in the region with statoliths compared to region without statolith (see Fig 4 c). The other main parameter controlling the gravitropic response is the pool number $\mathcal{P}$, where $\mathcal{P} \gg 1$ correspond to the infinite-pool regime and $\mathcal{P} \ll 1$ correspond to the limiting-pool regime (see Fig 4 b).

Once $\mathcal{R}$ and $\mathcal{P}$ are set, the final step is to compute how the different surfaces covered (and not covered) by the statoliths vary as function of the inclination angle θ. To this end, one has to know the final position of statoliths when a cell is tilted. Recently, we address this question and showed that statoliths at the bottom of statocytes behave like an effective liquid on long timescale, due to the agitation of statoliths by the cell activity Bérut et al. (2018). Therefore, the final free surface of the statoliths pile is horizontal, as sketched in Fig. 3. This key feature of the flowing behavior of statoliths allows us to reduce the computation of the surfaces in (12, 13) to a purely geometrical problem that depends on three parameters: the angle of inclination θ, the aspect ratio of the cell H/W and the initial aspect ratio of the statolith pile H_0/W (see Fig. 3). The corresponding relationships are given in Appendix B.

Fig. 6 presents the typical steady gravitropic response $\tilde{\Delta}^{\text{steady}}(\theta)$ predicted by the model (12, 13, 14) as a function of θ, in the case of an infinite pool ($\mathcal{P} \gg 1$) or a limiting pool ($\mathcal{P} \ll 1$), and for two extreme values of $\mathcal{R}$: $\mathcal{R} \simeq 1$ (red curve, low influence of statoliths on PIN binding) and $\mathcal{R} \gg 1$ (blue curve, strong influence of statoliths on PIN binding). The geometry used for the cell aspect ratio and the statoliths pile

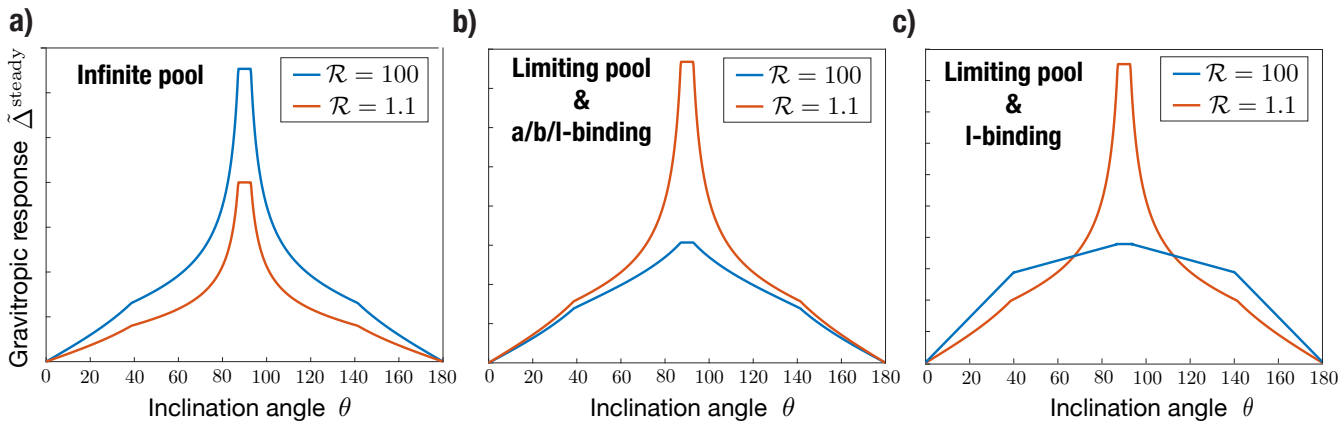

Figure 6. Steady gravitropic response $\tilde{\Delta}^{\text{steady}}$ (arbitrary amplitude) as a function of the inclination angle θ, for $\mathcal{R}$ either large or close to 1, in the case of (a) infinite pool ($\mathcal{P} \gg 1$), (b) limiting pool ($\mathcal{P} \ll 1$) with apical/basal/lateral binding, (c) limiting pool ($\mathcal{P} \ll 1$) with lateral binding only. Note that in the case of an infinite pool, results are the same in the a/b/l-binding or l-binding case. Geometrical parameters used are $H_0 = 4d$, $W = 10d$, $H = 25d$ where d stands for the diameter of a statolith.

ratio is taken from experimental observations of wheat coleoptile statocytes, with a typical aspect ratio $H/W = 2.5$ and $H_0/W = 1/2.5$. In the case of an infinite pool (Fig. 6 a), the gravitropic response presents a convex shape with a strong peak close to $90°$ whatever the value of $\mathcal{R}$, in disagreement with the usual sine-law. The amplitude of this peak is related to the cell geometry: the more elongated the cell, the higher the peak ; this is because more lateral surface is available for PIN attachment, without any limitation on the quantity of PIN in the infinite-pool regime (no dilution, see Fig 4 b). By contrast, in the limiting-pool case (Fig. 6 b,c), the response strongly depends on $\mathcal{R}$, the peak at $90°$ being much smaller for $\mathcal{R} \gg 1$ than for $\mathcal{R} \simeq 1$. Interestingly, the response in this case also depends on whether PIN can attach on every sides of the cell (apical/basal/lateral binding) or only on the lateral sides (lateral binding case), as attachment to the 'useless' apical and basal sides contribute to deplete PIN from the available pool. Overall, we see that only one case is compatible with the concave 'sine-law' shape observed experimentally: a limiting pool of PIN with lateral binding and $\mathcal{R} \gg 1$ (blue curve in Fig. 6 c).

In the following, we thus assume that PIN recycling occurs in the limited-pool regime ($\mathcal{P} \gg 1$), with lateral binding only. In this limit, and using expression of the surfaces given in Appendix B, the steady gravitropic response given by eqs. (12, 13, 14) can be written as:

$$\tilde{\Delta}^{\text{steady}}(\theta) = \frac{1}{2}\mathcal{A}(\mathcal{R}-1)\begin{cases} \dfrac{W\tan\theta}{2H + 2(\mathcal{R}-1)H_0} & \text{if} \quad W\tan\theta < 2H_0 \\ \dfrac{\sqrt{2H_0 W\tan\theta}}{2H + (\mathcal{R}-1)\sqrt{2H_0 W\tan\theta}} & \text{if} \quad 2H_0 < W\tan\theta < H^2/(2H_0) \\ \dfrac{1}{\mathcal{R}+1} & \text{else} \end{cases} \tag{15}$$

where the different conditions stand for cases where statoliths are totally absent left side, or totally covering the right side (see Fig. 7) and $\mathcal{A} = \frac{\alpha N_{\text{tot}} N}{\beta \int [ABCB]}$. Once the geometry of the cell and of the statoliths pile are fixed, the predicted gravitropic response depends on two dimensionless parameters: $\mathcal{R}$ and $\mathcal{A}$. Fig. 7 presents the experimental measurements of the 'sine-law' obtained by Chauvet et al. (2016) on wheat coleoptiles, together with the best fit of the (noisy) data using a least-square method. Reasonable agreement between theory and experiments is obtained with $\mathcal{R} \simeq 25$ and $\mathcal{A} \simeq 1.3$. It is interesting to note that within

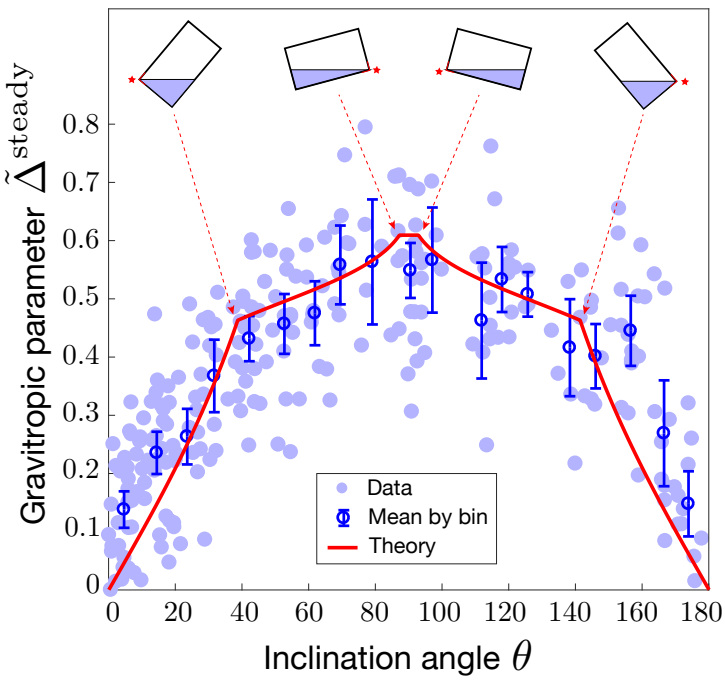

Figure 7. Modified sine-law $\tilde{\Delta}^{\text{steady}}$ as a function of the inclination angle θ. Comparison between the model prediction for $\mathcal{P} \ll 1$ (limiting pool) and l-binding (eq. (15) with $\mathcal{R} = 25$ and $\mathcal{A} = 1.3$, red line) and experiments on wheat coleoptiles (symbols, Chauvet et al. (2016)). Geometrical parameters used in the model for the statocyte are $H_0 = 4d$, $W = 10d$, $H = 25d$ where d stands for the diameter of a statolith. Errorbars are the mean value of the data by binning the [0,180] interval into 20 boxes.

our position-sensor framework, the predicted steady gravitropic response is not a simple 'sine-law', but rather a piece-wise curve with an overall concave shape. This law is also not universal and can be affected by several anatomical and physiological properties, such as the geometry of the cell H/W, the amount of statoliths H_0/W, or the molecular signaling machinery (embedded in the parameters $\mathcal{R}$ and $\mathcal{A}$).

3.2 Transient gravitropic response: dose-response law

The previous results deal with the steady gravitropic response obtained when the gravity stimulus (the angle of inclination θ) is permanent. We now turn to the study of the transient gravitropic response, i.e., when the system has not yet reached the steady state. This situation typically corresponds to 'dose-response' like experiments, in which the gravity stimulus is applied during a transient time ΔT only. Using such protocol on wheat coleoptiles, Chauvet et al. (2019) revealed the existence of an intrinsic 'memory' time τ_{memory} in the gravitropic response. For $\Delta T \gg \tau_{\text{memory}}$, the response was constant and equal to the steady response $\tilde{\Delta}^{\text{steady}}$. However, for $\Delta T \lesssim \tau_{\text{memory}}$, the response was smaller and became proportional to ΔT (Fig. 8). The memory time $\tau_{\text{memory}} \sim 15$ min identified in these experiments was longer than the sediment time of statoliths (~ 2 min) but shorter than the growth timescale (hours). It thus reflects a temporal process in the gravitropic signaling pathway that remains to be identified. We address below this question in the framework of the model.

The set of equations (5)-(7) give a complete description of the transient gravitropic response (we assume that sedimentation of statoliths is fast enough that the surfaces in (7) can be computed from their equilibrium values – see Appendix B). Two different typical times control the dynamics: τ_{aux}, describing the transport of auxin across the tissue of length $2R$, and τ_{PIN}, describing the dynamics of PIN at molecular scale. The

time scale associated to auxin transport $\tau_{\rm aux}$ can be estimated using eq. (5) for a constant coefficient of diffusion $\mathcal{D}$ and transport velocity v (i.e., PIN distribution). In this case, relaxation towards the stationary profile eq. (8) is exponential and occurs on a time scale set by the inverse of the shortest non-vanishing eigen-mode of equation (5):

$$\tau_{\rm aux} = \frac{1}{\pi^2 + ({\rm Pe}^2/4)} \times \frac{(2R)^2}{\mathcal{D}} \tag{16}$$

with ${\rm Pe} = (2Rv)/\mathcal{D}$ Mohsen and Baluch (1983). Estimating the Peclet number from the steady gravitropic response (${\rm Pe} = 2\tilde{\Delta}^{\rm steady} \approx 1$, see Fig. 7), and the auxin transport speed v from measurements of the speed of auxin pulses in plant tissues ($v \simeq 3\mu ms$, Goldsmith (1977); Rashotte et al. (2003)), gives $\tau_{\rm aux} \simeq 30s$ (we take $2R \sim 1$ mm). This is much shorter than the memory time $\tau_{\rm memory} \sim 15$ min evidenced in dose-response experiments, and even not larger than the statoliths sedimentation time. This suggests that the dynamics of the gravitropic response is controlled by $\tau_{\rm PIN}$, rather than by the auxin diffusion time $\tau_{\rm aux}$.

The time scale $\tau_{\rm PIN}$ is set by the slowest characteristic time of the system Eq. (7) describing PIN dynamics. From the eigenvalues of this linear system, those two time scales are obtained, which are solutions of:

$$\begin{aligned} &\tau^{-2} - (k_{\rm off,0} + k_{\rm off,1} + [k_{\rm on,0}S_0 + k_{\rm on,1}S_1]/N_{\rm tot})\tau^{-1} \\ &+(k_{\rm off,0} + k_{\rm on,0}S_0/N_{\rm tot})(k_{\rm off,1} + k_{\rm on,1}S_1/N_{\rm tot}) - k_{\rm on,0}k_{\rm on,1}S_0S_1/N_{\rm tot}^2 = 0\,. \end{aligned} \tag{17}$$

In the limiting pool case ($N_{\rm tot}k_{\rm off,i}/k_{\rm on,i}S_i \ll 1$), the two solutions are:

$$\tau_1 = \frac{N_{\rm tot}}{k_{\rm on,0}S_0 + k_{\rm on,1}S_1} \qquad \text{and} \qquad \tau_2 = \frac{k_{\rm on,0}S_0 + k_{\rm on,1}S_1}{k_{\rm off,0}k_{\rm on,1}S_1 + k_{\rm off,1}k_{\rm on,0}S_0}, \tag{18}$$

with $\tau_1 \ll \tau_2$. Therefore, the slowest time scale of the gravitropic signaling pathway, which sets $\tau_{\rm memory}$, should be given by $\tau_{\rm PIN} = \tau_2$. Note that when preferential attachment in region with statolith is achieved via a strongly increased attachment rate ($k_{\rm on,1} \gg k_{\rm on,0}$) and not by change of detachment rate ($k_{\rm off,0} \simeq k_{\rm off,1}$) we have $\tau_{\rm PIN} = k_{\rm off}^{-1}$. Conversely, if it is achieved by decreased detachment rate ($k_{\rm off,0} \gg k_{\rm off,1}$) and not by change of attachment rate ($k_{\rm on,0} \simeq k_{\rm on,1}$) we have $\tau_{\rm PIN} = k_{\rm off,0}^{-1}(1 + S_1/S_0) \simeq k_{\rm off,0}^{-1}$. Remarkably, in this last case, the equilibration time of PIN is not controlled by the slowest rate of detachment ($k_{\rm off,1}$), but by the fastest one ($k_{\rm off,0}$), due to the limiting pool.

To check these predictions, we solve the model for a transient gravitropic stimulus that reproduces the protocol of Chauvet et al. (2019). The inclination θ is set to 45° for a transient time ΔT and then put back to zero, the gravitropic response being defined as the maximal auxin gradient reached during the dynamics: $\tilde{\Delta}^{\rm trans} = {\rm Max}[\frac{c_{\rm bottom}(t) - c_{\rm top}(t)}{2c_{\rm mean}}]$. Fig. 8)(a) compares the experimental data of Chauvet et al. (2019) with the prediction of the model for $\tau_{\rm aux}/\tau_{\rm PIN} \ll 1$, using the parameters $\mathcal{R}$ and $\mathcal{A}$ already fixed by the steady response (see Fig. 7). Good agreement is obtained using $\tau_{\rm PIN} = 13$ min as the only fitting parameter. This result shows that τ_{PIN} is playing the role of the memory time evidenced by the experiments of Chauvet et al. (2019). If $\Delta T \ll \tau_{\rm PIN}$, PIN-transporters have not enough time to rearrange before the end of the stimulus, and the response is weak. Conversely if $\Delta T \gg \tau_{\rm PIN}$, PIN have time to rearrange and reach their steady repartition before the end of the stimulus, and the response is maximal, similar to the one of a permanent stimulus.

We finish our analysis by investigating the full temporal dynamics of the gravitropic response after a sudden inclination $\theta = 50°$. Fig. 8(b) presents the time evolution of the shoot curvature $\mathcal{C}(t)$ (or similarly $\theta_{tip}(t)$ for small curvatures) predicted by the model for $\tau_{\rm PIN} = 13$ min (blue curve), together with the

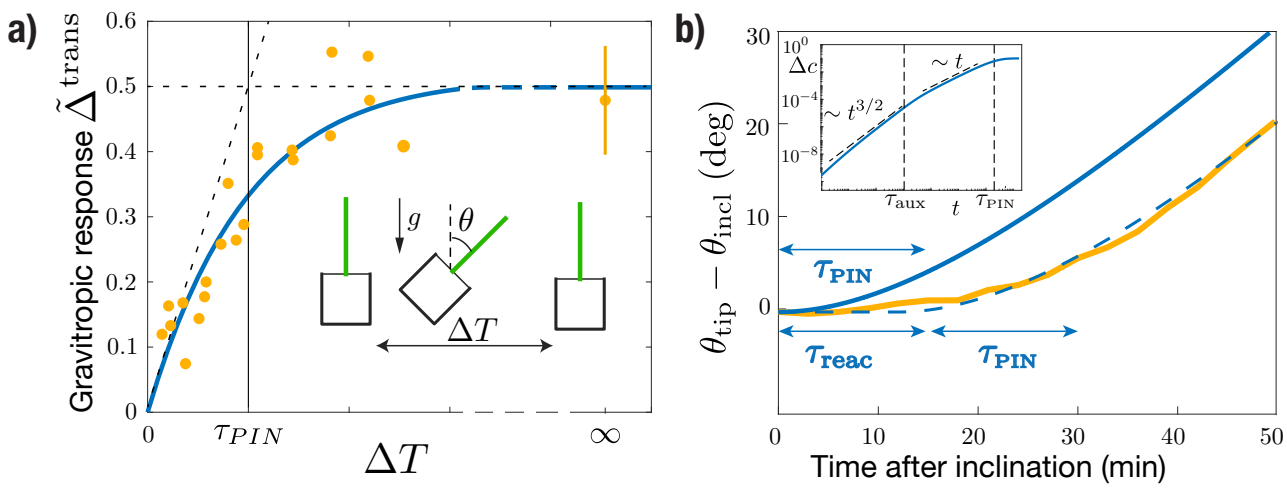

Figure 8. Gravitropic response to a transient inclination (dose-response like protocol). (a) Maximal gravitropic response reached during the dynamics as function of the inclination time ΔT for $\theta = 45°$. The blue solid line is the model prediction using $\tau_{\text{PIN}} = 13$ min ($\tau_{\text{aux}}/\tau_{\text{PIN}}$ and $\tau_1/\tau_{\text{PIN}} \ll 1$, other parameters are fixed as in Fig. 7). Symbols correspond to the aggregation results of (Chauvet et al., 2019) under $1g$ and $3g$. (b) Evolution of the tip angle after an inclination $\theta = 50°$ predicted by the model with the same parameters (blue solid line) and in the experiments of Chauvet et al. (2016) (orange thick line). The predicted model must be shifted by a constant time $\tau_{\text{reac}} = 13$ min (thin red line) to match the experimental curve. Inset: early time behavior of the gravitropic response predicted by the model in log-log scale.

experimental data of Chauvet et al. (2016) (yellow curve). The time scale of the curvature change τ_{PIN} is well captured by the model. However, to match the experiments, the model has to be shifted in time by a constant time $\tau_{\text{reac}} \approx 13$ min. Such delay or reaction time of the gravitropic response after the stimulus was already noticed by Chauvet et al. (2019), but does not seem described by the model. Actually, a careful analysis of the temporal behavior of the model (assuming $\tau_1 \ll \tau_{\text{aux}} \ll \tau_{\text{PIN}} = \tau_2$) shows that the auxin gradient at early times increases as $\Delta c \sim t^{3/2}$ (so that $\mathcal{C} \propto \int_0^t \Delta c dt \propto t^{5/2}$) as long as $t < \tau_{\text{aux}}$, before varying as $\Delta c \sim t$ for $\tau_{\text{aux}} < t < \tau_{\text{PIN}}$ (Inset of Fig. 8 b). These scaling laws are thus not compatible with a very flat initial response.

4 DISCUSSION

In this paper, we have derived a multi-scale model of plant gravitropism which links the different steps of the gravitropic signaling pathway: (i) the initial intracellular perception of gravity by statoliths, (ii) the transduction of this physical signal into a biochemical signal through the reorganization of PINs at the membrane of statocytes, (iii) the intercellular signal transmission via auxin transport and (iv) asymmetric organ growth. The main originality of the model lies in the mechanistic link we propose between the statoliths position and the dynamics of PIN, based on the recent position-sensor hypothesis (Pouliquen et al., 2017). Remarkably, this basic assumption coupled to auxin transport and growth in an idealized tissue made of a one-dimensional array of cells recovers several major features of the gravitropic response of plants.

4.1 A new interpretation of the sine-law of plant gravitropism

The first main result concerns the steady gravitropic response to a permanent gravity stimulus, $\tilde{\Delta}^{\text{steady}}(\theta)$. For many plants, this response takes the form of an inclination-dependent law with a sine-like shape, called for this reason the sine-law of plant gravitropism (Sachs, 1887; Larsen, 1969; Iino et al., 1996; Galland, 2002; Dumais, 2013). This sine-law has long been interpreted in terms of a force sensor mechanism, for

the projected weight of the statoliths on the lateral surface of the cell varies with the sine of the inclination angle (Audus, 1969; Barlow, 1995). However, recent experiments showing that the response is independent of the gravity intensity have dismissed this force-sensing hypothesis, calling for a new interpretation of the sine law (Chauvet et al., 2016; Pouliquen et al., 2017). Importantly, our model predicts a steady gravitropic response $\tilde{\Delta}^{\text{steady}}(\theta)$ dependent on the inclination angle, but without invoking any force-based mechanisms. In the model, the initial gravitropic stimulus is the statoliths position at the cell membrane, which modifies the trafficking of PIN at the cell membrane. Since statoliths behave like a liquid (Bérut et al., 2018), their position in steady state is a purely geometrical cue, which depends only on the cell inclination not on the statoliths weight. As a result, the gravitropic response predicted by the model depends on the inclination but not on the gravity intensity, in agreement with the observations.

In the model, the actual shape of the gravitropic response $\tilde{\Delta}^{\text{steady}}(\theta)$ is never a pure sine law and critically depends on several parameters related either to geometric factors (aspect ratio of the statocytes, aspect ratio of the sedimented statoliths pile) or to molecular processes (parameter $\mathcal{R}$ characterizing the intensity of coupling between statolith position and PIN, parameter $\mathcal{P}$ characterizing the number of PIN available inside the cell, parameter $\mathcal{A}$ characterizing the ratio between the conductance of PIN carriers to the total conductance of auxin transporters). For elongated cells and shallow statoliths piles such as those of the wheat coleoptile statocytes, the shape of the response approaches a sine-shape only in the case of a strong coupling between statoliths and PIN ($\mathcal{R} \gg 1$), and for a number of PINs conserved along the cell membrane (limiting pool regime, $\mathcal{P} \ll 1$). This latter assumption is common in models of auxin transport (Runions et al., 2014; Retzer et al., 2019), while the strong coupling assumption is compatible with the large asymmetry in PIN localization observed upon gravity stimulation (Friml et al., 2002; Harrison and Masson, 2008; Kleine-Vehn et al., 2010). Interestingly, although gravity is absent from the model, the gravitropic response may depend on the amount of statoliths, through the geometrical aspect ratio of the statoliths pile H_0/W. Therefore, the model could account for experiments performed on starch-less and starch-excess mutants, which shows a modified response when the number of statoliths is changed (Kiss et al., 1997; Vitha et al., 2007; Pouliquen et al., 2017). Finally, it is worth noting that the model assumes that the statoliths form a static pile at the bottom of the cell, while statoliths exhibit a dynamic and random agitation due to the interaction with the cytoskeleton (Sack et al., 1986; Saito et al., 2005; Nakamura et al., 2011; Bérut et al., 2018). We might expect that this agitation reduces the averaged contact time between the statoliths and the cell membrane, therefore decreasing the coupling between statoliths and PIN. It would be interesting to extend the model in order to incorporate such effect of agitation on the gravitropic response. The model could then be compared with the behavior of agravitropic mutants in *Arabidopsis thaliana* like *sgr9*, whose weaker response is likely associated to an abnormally strong agitation of its statoliths (Nakamura et al., 2011).

Overall, these results suggests that the classical sine-law of plant gravitropism might not be universal, as its shape and amplitude in the model depend on several anatomical and physiological parameters. Full measurements of the gravitropic response of plants over a wide range of inclination are scarce and mostly performed on shoot coleoptiles. It would be interesting to perform systematic measurements of the sine-law on other plant organs like roots or stem, where different statocytes geometry and tissue organization are encountered.

4.2 The gravity-independent memory process in dose-response laws is likely associated to PIN dynamics

The second main result of our study concerns the gravitropic response to a transient gravity stimulus. For a sudden inclination applied at time $t = 0$, the model predicts that the response reaches the steady response

$\tilde{\Delta}^{\text{steady}}(\theta)$ only after a time large compared to a 'memory' timescale τ_{memory}, corresponding to the slowest timescale of introduced in the model. Therefore, when the stimulus is applied only during a transient time $\Delta T < \tau_{\text{memory}}$, a weaker gravitropic response is observed, which follows a dose-response like law. In the model, this memory time is not associated with the sediment time of the statoliths, which was assumed much shorter than the other timescales of the gravitropic signaling pathway (a valid assumption on Earth gravity). Our model is therefore compatible with the recent experiments of Chauvet et al. (2019) performed on wheat coleoptiles, showing a dose-like behavior of the gravitropic response with a memory time τ_{memory} independent of gravity. It also provides the explicit origin of this memory process, which was postulated in the model of Chauvet et al. (2019). In our model, two different processes can filter the signal of the statoliths position: auxin transport across the tissue and the dynamics of PIN cycling at the molecular scale. Our study suggests that the limiting process is controlled by PIN dynamics, such that $\tau_{\text{memory}} = \tau_{\text{PIN}}$, auxin transport being is too fast to account for the memory time measured experimentally ($\sim$ 10-20 min). Interestingly, visualization of the PIN3 auxin efflux carrier in root columella cells after a sudden change in the gravity vector indicates a time scale of about 10 min for complete relocation (Friml et al., 2002), a duration very close to the memory time measured by (Chauvet et al., 2019). Although our model successfully captures the existence and origin of a gravity-independent memory process in the signaling pathway, it is not able to describe the delay time $\tau_{\text{reaction}} \sim 10$ min observed between the application of the stimulus and the first gravitropic response (Chauvet et al., 2019). We might rationalize it as the time needed to reorganize the cytoskeleton implied in the transport of PIN carriers, the time needed by a PIN to go from the pool towards the plasma membrane, or the time of incorporation of a PIN into the membrane. It is worth noting that a similar timescale of about 10 min was identified in the gravity-sensing columella cells for the internalization of PIN3 from the plasma membrane into vesicles (Kleine-Vehn et al., 2010). To confirm this key role of PIN dynamics in the gravitropic response, further experiments combining a transient gravitropic stimulus with pharmacological and genetic approaches are needed.

4.3 Back to the statoliths/PIN coupling assumption

We conclude by discussing the possible origin of the coupling between statoliths and PIN carriers, which is at the core of our model. Although the respective roles of statoliths and PIN auxin transporters in plants gravitropism are now well established, the link between the two is still not clear (see Nakamura et al. (2019) for a recent review of the possible molecular actors involved). In this article, we have used a very general hypothesis for this coupling based on the recent finding that the relevant gravitropic stimulus is the statoliths position inside the gravisensing cells (Chauvet et al., 2016; Pouliquen et al., 2017; Bérut et al., 2018). We have postulated that statoliths in contact with the cell membrane bias the exocytosis and endocytosis rate of PIN recycling, therefore inducing an asymmetry of PIN distribution when statoliths reposition in response to plant inclination. Our results suggests that this interaction between PIN and statoliths is strong, as large values of the parameter $\mathcal{R}$ characterizing the ratio of exo and endocytosis rates with and without statoliths are needed to match the experimental gravitropic response. This interaction between statoliths and PIN could be achieved by different mechanisms. Statoliths could modify PIN vesicle-mediated transportation to the membrane, for example by modifying the architecture of the actin cytoskeleton. Another possibility would be that internalization of PIN from the membrane is reduced by the presence of statoliths, for example by simple steric effects. Indeed, direct visualization of PIN internalization reveals a length scale of $\sim 1\,\mu$m for the endosome formation, not far from the statolith size (Kleine-Vehn et al., 2010). A last possibility could be that PIN carriers cluster in the region without statoliths and not in region with. Indeed, for a conserved number of PIN proteins, clustering reduces the efficiency of efflux, as this diffusion process scales not linearly but as the square-root of the number of carriers Bénichou and Voituriez (2014); Valet et al. (2019). Such clustering has been highlighted Kleine-Vehn et al. (2011), but, to our knowledge, no

comparison has been done between regions with and without statoliths. Discriminating between these molecular mechanisms would require advanced molecular biology studies, and is much beyond the scope of this paper.

CONFLICT OF INTEREST STATEMENT

The authors declare that the research was conducted in the absence of any commercial or financial relationships that could be construed as a potential conflict of interest.

AUTHOR CONTRIBUTIONS

N.L., O.P., and Y.F. designed research. N.L. built and analyzed the model with inputs from O.P. and Y.F. N.L., O.P., and Y.F. wrote the paper..

FUNDING

This work was supported by the European Research Council (ERC) under the European Union's Horizon 2020 research and innovation programme (grant agreement N°647384) and by the French National Agency (ANR) under the program Blanc Grap2 (ANR-13-BSV5-0005-01).

ACKNOWLEDGMENTS

The authors would like to thank Valérie Legué and Bruno Moulia for the many stimulating discussions we have continually had on this subject.

APPENDIX A: CASE OF STATOLITHS ONLY PRESENT ON A RING

Let be a central region between l and $2R-l$ with no statolith (and constant efflux rate P_0). We can redo the calculation leading to (4) in this geometry. Clearly, equations will be similar in each region, with $v=0$ in the central one. We have to take care to the continuity of the flux at the jonction of each regions. We can show that $J(l)=(P+\delta P)c(l^-)-P_0c(l^+)$ and $J(2R-l)=P_0c((2R-l)^-)-Pc((2R-l)^+)$. At steady state, we thus get a jump of auxin concentration: $c(l^+)=(P+\delta P)/P_0\ c(l^-)$ and $c((2R-l)^+)=P_0/P\ c((2R-l)^-)$. In the limit of small Peclet number, we thus get $\Delta c/c=(P_0/P)(vl/\mathcal{D})$.

APPENDIX B: EXPRESSION OF THE GEOMETRIC PARAMETERS AS A FUNCTION OF θ

We give here the value of the surfaces $S_i^{r,l}(\theta)$ that are necessary to compute the Peclet number as a function of the angle (see Eq. (15)). As statoliths are solid, the shaded area in 3 is conserved and is thus equal to H_0W. We note $\theta_1=\arctan 2H_0/W$ the angle for which the horizontal level meets the lower left corner, and $\theta_2=\arctan H^2/(2H_0W)$ the one for which it meets the upper right one (we assume $H_0<H/2$). Elementary geometry calculations give:

$$S_0^l=\begin{cases} H-H_0+\dfrac{W\tan\theta}{2} & \text{if} \quad \theta<\theta_1 \\ H \quad \text{else} \end{cases} \tag{19}$$

$$S_1^l=\begin{cases} H_0-\dfrac{W\tan\theta}{2} & \text{if} \quad \theta<\theta_1 \\ 0 \quad \text{else} \end{cases} \tag{20}$$

$$S_0^r = \begin{cases} H - H_0 - \dfrac{W \tan\theta}{2} & \text{if} \quad \theta < \theta_1 \\ H - \sqrt{2H_0 W \tan\theta} & \text{if} \quad \theta_1 < \theta < \theta_2 \\ 0 \quad \text{else} \end{cases} \tag{21}$$

$$S_1^r = \begin{cases} H_0 + \dfrac{W \tan\theta}{2} & \text{if} \quad \theta < \theta_1 \\ \sqrt{2H_0 W \tan\theta} & \text{if} \quad \theta_1 < \theta < \theta_2 \\ H \quad \text{else} \end{cases} \tag{22}$$

In the case of apical binding, this leads to

$$S_0 = \begin{cases} 2(H - H_0) & \text{if} \quad \theta < \theta_1 \\ 2H - \sqrt{2H_0 W \tan\theta} & \text{if} \quad \theta_1 < \theta < \theta_2 \\ H \quad \text{else} \end{cases} \tag{23}$$

$$S_1 = \begin{cases} 2H_0 & \text{if} \quad \theta < \theta_1 \\ \sqrt{2H_0 W \tan\theta} & \text{if} \quad \theta_1 < \theta < \theta_2 \\ H \quad \text{else} \end{cases} \tag{24}$$

In the case of apical/basal/lateral binding, the expressions for the total surfaces are slightly modified due to attachment at apical and basal side.

SUPPLEMENTAL DATA

Supplementary Material should be uploaded separately on submission, if there are Supplementary Figures, please include the caption in the same file as the figure. LaTeX Supplementary Material templates can be found in the Frontiers LaTeX folder.

DATA AVAILABILITY STATEMENT

The datasets [GENERATED/ANALYZED] for this study can be found in the [NAME OF REPOSITORY] [LINK].

REFERENCES

[Dataset] Audus, L. (1969). The physiology of plant growth and development chap. geotropism, 203–241

Band, L. R., Wells, D. M., Larrieu, A., Sun, J., Middleton, A. M., French, A. P., et al. (2012). Root gravitropism is regulated by a transient lateral auxin gradient controlled by a tipping-point mechanism. *Proceedings of the National Academy of Sciences* 109, 4668

Barlow, P. W. (1995). Gravity perception in plants: a multiplicity of systems derived by evolution? *Plant, Cell & Environment* 18, 951–962

Bastien, R., Bohr, T., Moulia, B., and Douady, S. (2013). Unifying model of shoot gravitropism reveals proprioception as a central feature of posture control in plants. *Proceedings of the National Academy of Sciences* 110, 755–760

Bastien, R., Douady, S., and Moulia, B. (2014). A unifying modeling of plant shoot gravitropism with an explicit account of the effects of growth. *Frontiers in plant science* 5, 136

Bénichou, O. and Voituriez, R. (2014). From first-passage times of random walks in confinement to geometry-controlled kinetics. *Physics Reports* 539, 225–284

Bérut, A., Chauvet, H., Legué, V., Moulia, B., Pouliquen, O., and Forterre, Y. (2018). Gravisensors in plant cells behave like an active granular liquid. *Proceedings of the National Academy of Sciences* 115, 5123

Chauvet, H., Moulia, B., Legué, V., Forterre, Y., and Pouliquen, O. (2019). Revealing the hierarchy of processes and time-scales that control the tropic response of shoots to gravi-stimulations. *Journal of Experimental Botany* 70, 1955–1967

Chauvet, H., Pouliquen, O., Forterre, Y., Legué, V., and Moulia, B. (2016). Inclination not force is sensed by plants during shoot gravitropism. *Scientific reports* 6, 35431–35431

Chelakkot, R. and Mahadevan, L. (2017). On the growth and form of shoots. *Journal of The Royal Society Interface* 14, 20170001

Dumais, J. (2013). Beyond the sine law of plant gravitropism. *Proceedings of the National Academy of Sciences* 110, 391–392

Dyson, R. J., Vizcay-Barrena, G., Band, L. R., Fernandes, A. N., French, A. P., Fozard, J. A., et al. (2014). Mechanical modelling quantifies the functional importance of outer tissue layers during root elongation and bending. *New Phytologist* 202, 1212–1222

Fendrych, M., Akhmanova, M., Merrin, J., Glanc, M., Hagihara, S., Takahashi, K., et al. (2018). Rapid and reversible root growth inhibition by tir1 auxin signalling. *Nature plants* 4, 453–459

Friml, J., Wiśniewska, J., Benková, E., Mendgen, K., and Palme, K. (2002). Lateral relocation of auxin efflux regulator pin3 mediates tropism in arabidopsis. *Nature* 415, 806–809

Galland, P. (2002). Tropisms of avena coleoptiles: sine law for gravitropism, exponential law for photogravitropic equilibrium. *Planta* 215, 779–784

Galston, A. W. and Hand, M. E. (1949). Studies on the physiology of light action; auxin and the light inhibition of growth. *Am J Bot* 36, 85–94

Goldsmith, M. H. M. (1977). The polar transport of auxin. *Annual Review of Plant Physiology* 28, 439–478

Grieneisen, V. A., Scheres, B., Hogeweg, P., and M Marée, A. F. (2012). Morphogengineering roots: comparing mechanisms of morphogen gradient formation. *BMC Systems Biology* 6, 37

Harrison, B. R. and Masson, P. H. (2008). Arl2, arg1 and pin3 define a gravity signal transduction pathway in root statocytes. *The Plant Journal* 53, 380–392

Hopkins, W. G. and Hüner, N. P. (2009). *Introduction to Plant Physiology 4th ed*

Iino, M., Tarui, Y., and Uematsu, C. (1996). Gravitropism of maize and rice coleoptiles: dependence on the stimulation angle. *Plant, cell & environment* 19, 1160–1168

Kiss, J. Z., Guisinger, M. M., Miller, A. J., and Stackhouse, K. S. (1997). Reduced gravitropism in hypocotyls of starch-deficient mutants of arabidopsis. *Plant and Cell Physiology* 38, 518–525

Kleine-Vehn, J., Ding, Z., Jones, A. R., Tasaka, M., Morita, M. T., and Friml, J. (2010). Gravity-induced pin transcytosis for polarization of auxin fluxes in gravity-sensing root cells. *Proceedings of the National Academy of Sciences* 107, 22344–22349

Kleine-Vehn, J. and Friml, J. (2008). Polar targeting and endocytic recycling in auxin-dependent plant development. *Annual Review of Cell and Developmental Biology* 24, 447–473

Kleine-Vehn, J., Wabnik, K., Martinière, A., Łangowski, Ł., Willig, K., Naramoto, S., et al. (2011). Recycling, clustering, and endocytosis jointly maintain pin auxin carrier polarity at the plasma membrane. *Molecular systems biology* 7, 540–540

Kramer, E. M., Frazer, N. L., and Baskin, T. I. (2007). Measurement of diffusion within the cell wall in living roots of arabidopsis thaliana. *Journal of experimental botany* 58, 3005–3015

Krecek, P., Skupa, P., Libus, J., Naramoto, S., Tejos, R., Friml, J., et al. (2009). The pin-formed (pin) protein family of auxin transporters. *Genome biology* 10, 249–249

Kutschera, U. and Niklas, K. (2007). The epidermal-growth-control theory of stem elongation: an old and a new perspective. *Journal of plant physiology* 164, 1395–1409

Larsen, P. (1969). The optimum angle of geotropic stimulation and its relation to the starch statolith hypothesis. *Physiologia Plantarum* 22, 469–488

Meroz, Y., Bastien, R., and Mahadevan, L. (2019). Spatio-temporal integration in plant tropisms. *Journal of the Royal Society Interface* 16, 20190038

Mohsen, M. F. N. and Baluch, M. H. (1983). An analytical solution of the diffusion-convection equation over a finite domain. *Applied mathematical modelling* 7, 285–287

Morita, M. T. (2010). Directional gravity sensing in gravitropism. *Annual review of plant biology* 61, 705–720

Moulia, B. and Fournier, M. (2009). The power and control of gravitropic movements in plants: a biomechanical and systems biology view. *Journal of experimental botany* 60, 461–486

Nakamura, M., Nishimura, T., and Morita, M. T. (2019). Gravity sensing and signal conversion in plant gravitropism. *Journal of experimental botany* 70, 3495–3506

Nakamura, M., Toyota, M., Tasaka, M., and Morita, M. T. (2011). An arabidopsis e3 ligase, shoot gravitropism9, modulates the interaction between statoliths and f-actin in gravity sensing. *The Plant Cell* 23, 1830–1848

Pouliquen, O., Forterre, Y., Bérut, A., Chauvet, H., Bizet, F., Legue, V., et al. (2017). A new scenario for gravity detection in plants: the position sensor hypothesis. *Physical Biology* 14, 035005

Rashotte, A. M., Poupart, J., Waddell, C. S., and Muday, G. K. (2003). Transport of the two natural auxins, indole-3-butyric acid and indole-3-acetic acid, in arabidopsis. *Plant Physiology* 133, 761

Retzer, K., Akhmanova, M., Konstantinova, N., Malínská, K., Leitner, J., Petrášek, J., et al. (2019). Brassinosteroid signaling delimits root gravitropism via sorting of the arabidopsis pin2 auxin transporter. *Nature communications* 10, 1–15

Runions, A., Smith, R. S., and Prusinkiewicz, P. (2014). Computational models of auxin-driven development. In *Auxin and its role in plant development* (Springer). 315–357

Sachs, J. (1887). *Lectures on the Physiology of Plants* (Clarendon Press)

Sack, F. D., Suyemoto, M. M., and Leopold, A. C. (1986). Amyloplast sedimentation and organelle saltation in living corn columella cells. *American journal of botany* 73, 1692–1698

Saito, C., Morita, M. T., Kato, T., and Tasaka, M. (2005). Amyloplasts and vacuolar membrane dynamics in the living graviperceptive cell of the arabidopsis inflorescence stem. *The Plant Cell* 17, 548–558

Silk, W. K. (1984). Quantitative descriptions of development. *Ann. Rev. Plant Physiol.* 35, 479–518

Toyota, M. and Gilroy, S. (2013). Gravitropism and mechanical signaling in plants. *American journal of botany* 100, 111–125

Valet, M., Pontani, L.-L., Voituriez, R., Wandersman, E., and Prevost, A. M. (2019). Diffusion through nanopores in connected lipid bilayer networks. *Phys. Rev. Lett.* 123, 088101

Vitha, S., Yang, M., Sack, F. D., and Kiss, J. Z. (2007). Gravitropism in the starch excess mutant of arabidopsis thaliana. *American journal of botany* 94, 590–598

Zažímalová, E., Murphy, A. S., Yang, H., Hoyerová, K., and Hošek, P. (2010). Auxin transporterswhy so many? *Cold Spring Harbor perspectives in biology* 2, a001552